nature portfolio

Peer Review File

Achieving irradiation-resistant metallic alloys by immobilizing induced defects

Corresponding Author: Dr Shijun Zhao

This file contains all reviewer reports in order by version, followed by all author rebuttals in order by version.

Version 0:

Reviewer comments:

Reviewer #1

(Remarks to the Author)
This manuscript presents an interesting approach to designing irradiation-resistant alloys by exploiting lattice distortion. The combination of experimental characterization and computational modeling demonstrates, comparing with other three materials, the $Ni_{80}Mo_{20}$ alloy exhibits suppressed defect clustering under irradiation. The work also provides a framework to reconcile conflicting prior results in the literature and suggests a promising design pathway for radiation-tolerant structural materials. The manuscript is well written, and the results will be of significant interest to the nuclear materials community. It can be published after the authors address the following questions and suggestions:

1. The highest irradiation dose examined in this study is 0.43 DPA, which is relatively low for drawing conclusions about achieving superior irradiation resistance. Experimental data at higher doses (ideally >10 DPA) would be essential, which would substantially strengthen the quality and impact of the findings.

2. The modeling results (e.g., Fig. 3) and Figure 4a suggest that introducing distortion decreases the vacancy migration barrier while increasing the interstitial migration barrier, leading to enhanced recombination through barrier overlap. At the same time, the manuscript argues that lattice distortion traps both vacancies and interstitials (i.e., increases both migration barriers). This appears contradictory. It's noted that in the $Ni_{100-x}Mo_x$ series, increasing Mo content/distortion is shown to increase diffusivity, not reduce it. The authors should carefully reconcile these points and provide one clear mechanism.

3. Diffusion mechanisms are temperature dependent. The manuscript would be strengthened by either providing direct diffusion modeling results at 300 K (to match experimental conditions) or at least a more detailed mechanistic discussion of the differences between the 1000 K modeling results and the 300 K experiments.

Reviewer #3

(Remarks to the Author)
The aim of this paper is to tie local lattice distortion to the microstructural evolution of metallic alloys under irradiation.

In its current state, the article is not suitable for publication in Nature Communications without substantial revisions for the following reasons.

The work does not support several of the claims made. For example, in the introduction the claim is made that, "we demonstrate that superb irradiation-tolerant alloys can be achieved by effectively immobilizing irradiation-induced defects, including interstitials and vacancies, through maximizing lattice distortion effects" yet the work consists of room temperature ion irradiations to a peak damage of 0.43 dpa and modeling up to 0.01 dpa (at non-physical damage rates) with MD and 0.4 dpa with CRA. These temperatures and damage levels are far too low to be able to claim superb irradiation tolerance has been demonstrated as the experimental and simulated conditions are not sufficient to surpass the incubation period before extended defect (e.g., voids) can form. Similarly, it is stated that, "we present a new paradigm to design irradiation-resistant MPEAs through immobilizing both interstitials and vacancies by strategically engineering the degree of lattice distortion," however, many of the concepts presented have been studied at length, including by some of the co-authors, through the Energy Dissipation to Defect Evolution (EDDE) Energy Frontier Research Center EFRC over the last decade (e.g., references 18, 26, https://doi.org/10.1016/j.jnucmat.2019.03.031, https://doi.org/10.1038/ncomms9736).

More information is needed regarding the experimental methodology, including the dose rate for the ion irradiation, how the thickness of the TEM lamellae determined (in order to calculate dislocation densities), and how the dpa of the imaged locations was determined. The last point is relevant because the TEM micrographs in Fig 1 appear to show a monotonically decreasing damage depth while the SRIM calculations show NiFe having a greater depth than Ni80Mo20 and NiCoV having the greatest depth. This is relevant because if the implantation depths are substantially different, then the damage profiles are also substantially different (given similar fluence, material density, and displacement threshold energy which is assumed to be 40 eV for all elements).

From a formatting perspective, the article is overly reliant on supplementary materials. There are 20 references to the supplementary materials, often referring to critical information for the conclusions being drawn. If information is necessary to support the points being made, it needs to be included in the body of the article. Additionally, Supp. Fig. 5 has a typo in the X axis title.

Version 1:

Reviewer comments:

Reviewer #1

(Remarks to the Author)
1) This revised manuscript includes new irradiation experiments up to 10 DPA, significantly strengthening the original submission. The new high-dose data demonstrate that the effect of increased "lattice distortion" persists at elevated damage levels and continues to effectively suppress defect cluster size and density.

2) The role of "lattice distortion" in defect evolution is clarified, including the modification of migration barriers and the enhancement of correlation effects. The two-stage mechanism proposed by the authors clearly reconciles the effects on vacancy and interstitial diffusion.

3) As to the discussion of diffusion mechanisms at 1000 K vs. 300 K, it is said that the underlying mechanisms identified at 1000 K remain operative at 300 K, albeit at reduced jump frequencies. Given the broad distribution of migration barriers in concentrated alloys, lowering the temperature effectively selects the lower-barrier diffusion pathways while simultaneously enhancing correlation. Effective diffusion paths and migration modes can change with temperature, e.g., Nature Communications 15, 3879 (2024). The enhanced trapping observed at lower temperatures could originate from such diffusion-mode transitions. It may be helpful to clarify the manuscript, as it more precisely elucidates the temperature-dependent diffusion mechanisms.

Overall, this is an intriguing and technically solid study. By providing mechanistic insight into defect kinetics in chemically disordered alloys, this work offers a new perspective for rationalizing prior conflicting reports and a timely approach to designing radiation-tolerant alloys. The results will be of interest to the broad community, and publication in Nature Communications is therefore recommended!

Reviewer #3

(Remarks to the Author)
While qualifying the irradiation tolerance of the reported alloys as "superior" and "superb" is dubious after only modest irradiation doses at room temperature, the revised version of the paper is more relevant with the 10 dpa damage level than the prior 0.43 dpa studied. Similarly, it is difficult to assess just how immobilized the vacancies in the materials are, given that vacancies in most Ni-based alloys are effectively immobile at room temperature already. It remains to be seen whether the trends reported on will hold under reactor-relevant conditions, however the revised experiments and analysis may be included in the body of literature for the basis of discussion and future work.

Dear Editor and reviewers,

We sincerely thank you for providing us with the opportunity to revise our manuscript (manuscript number: NCOMMS-25-41925) entitled “*Achieving superior irradiation-resistant metallic alloys by immobilizing induced defects*”. We appreciate the editorial process and respect the reviewers’ insights. The meticulous reviews and insightful comments have been invaluable in improving our work.

In response to the constructive feedback, we have thoroughly revised the manuscript. Please find our point-by-point responses to each reviewer's comments below. The original report is given in *Calibri italic* font, and our response is in regular blue text. The revised texts in the manuscript are provided in red font. We believe these revisions represent a significant enhancement over the original submission. In accordance with the journal’s data availability requirements, we have provided the source data supporting the figures and tables in the manuscript. All the data is submitted in a single Excel file entitled “source_data.xlsx”.

We deeply appreciate your consideration of our manuscript and look forward to receiving good news from you. If you have any further queries, please do not hesitate to contact me.

Thank you very much and best regards,

Prof. Shijun Zhao
Department of Mechanical Engineering
City University of Hong Kong
Tat Chee Avenue, Kowloon Tong, Hong Kong, China
shijzhao@cityu.edu.hk

Reviewer 1

This manuscript presents an interesting approach to designing irradiation-resistant alloys by exploiting lattice distortion. The combination of experimental characterization and computational modeling demonstrates, comparing with other three materials, the $Ni_{80}Mo_{20}$ alloy exhibits suppressed defect clustering under irradiation. The work also provides a framework to reconcile conflicting prior results in the literature and suggests a promising design pathway for radiation-tolerant structural materials. The manuscript is well written, and the results will be of significant interest to the nuclear materials community. It can be published after the authors address the following questions and suggestions:

We express our sincere gratitude to the reviewer for the positive view of our work and thoughtful evaluation. We have carefully addressed each issue raised and have made revisions to our manuscript, as detailed below.

Comment 1.1: The highest irradiation dose examined in this study is 0.43 DPA, which is relatively low for drawing conclusions about achieving superior irradiation resistance. Experimental data at higher doses (ideally >10 DPA) would be essential, which would substantially strengthen the quality and impact of the findings.

Response 1.1: We thank the reviewer for this constructive comment regarding the irradiation dose range. To address this concern and assess defect evolution at higher irradiation levels, we have performed additional irradiation experiments up to 10 DPA, complemented by atomistic simulations using the creation–relaxation algorithm. The new results, presented in **Fig. 1** and **Supplementary Fig. 11**, demonstrate that increasing lattice distortion continues to effectively suppress both defect cluster size and density at elevated irradiation doses. These observations confirm that the proposed defect-immobilization mechanism remains operative under substantially high dose irradiation conditions, thereby strengthening the robustness and generality of our conclusions.

In the revised manuscript, we have replaced the previous discussion of **Fig. 1** with the new 10 DPA irradiation experiment, as follows:

Fig. 1a shows the cross-sectional distribution of dislocation loops along the depth for all materials post-irradiation, with images obtained under a two-beam condition (g = 200). The region of about 200 nm from the surface was removed due to “flash polishing” thinning. In addition, dislocation loop information from this region was excluded from the statistical analysis to minimize surface effects. Based on SRIM-2013 calculations (using the K-P mode and a displacement threshold energy of 40 eV for all elements), the damage range is approximately 1500 nm, with a peak damage level of about 10 displacement per atom (DPA). The corresponding damage profiles are provided in **Fig. 1b**.

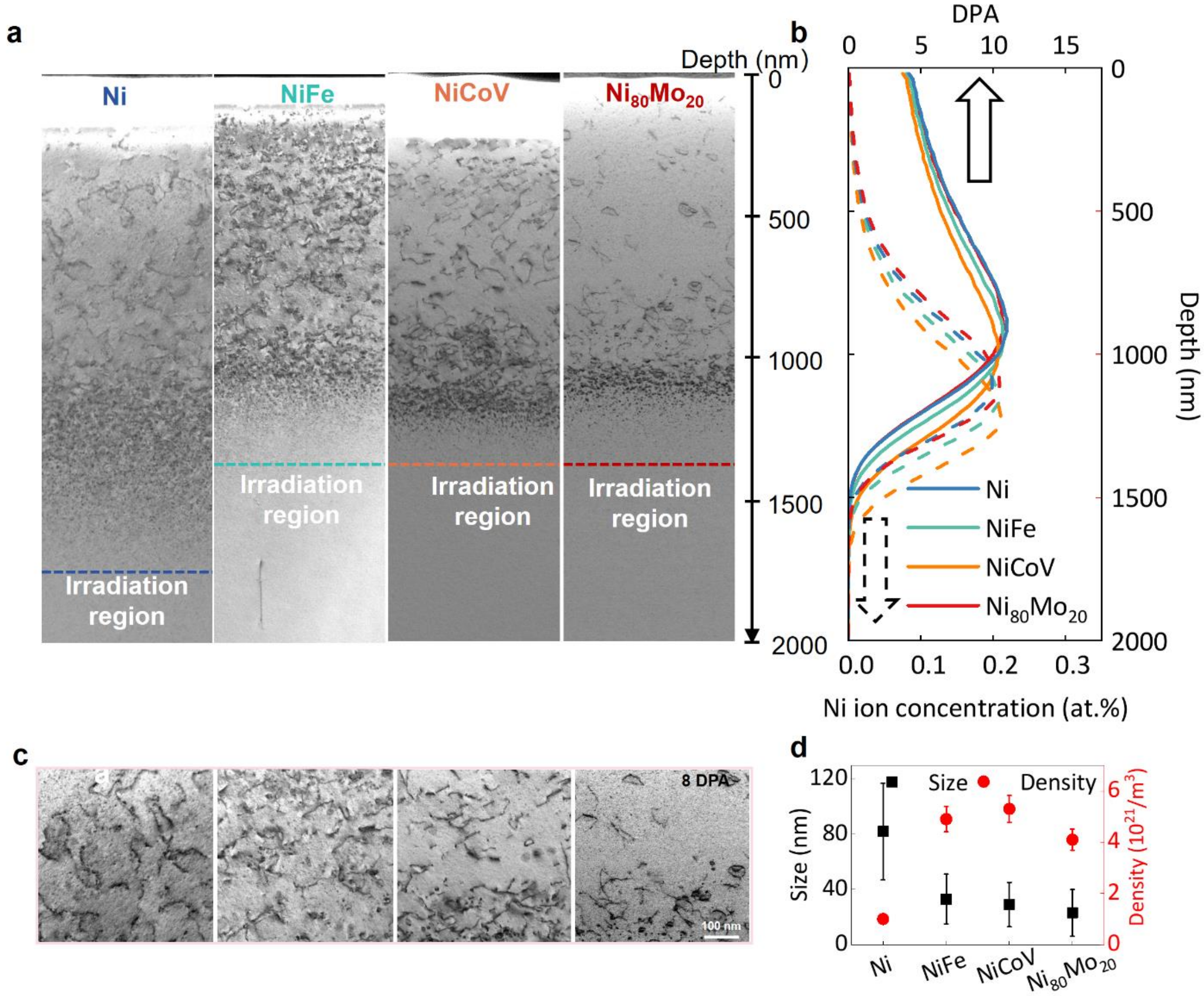

Fig. 1 | Irradiation response of Ni, NiFe, NiCoV, and $Ni_{80}Mo_{20}$ alloys exhibiting various degrees of lattice distortion after exposure to 3 MeV Ni^{+} ions at a fluence of 1×10^{16} ions/cm^2. a, Cross-sectional distribution of dislocation loops along depth after irradiation. **b,** The depth profiles of damage and implanted Ni concentration calculated using the SRIM-2013 software. **c,** Morphological characteristics of dislocation loops at 8 DPA. **d,** Comparison of the average size and density of dislocation loops across the entire irradiated area.

Observations at an irradiation dose of 8 DPA (**Fig. 1c**) reveal that dislocation loops in Ni and NiFe are almost exclusively glissile perfect loops, whereas a fraction of sessile faulted loops is present in NiCoV and $Ni_{80}Mo_{20}$, indicating that the growth of dislocation loops is suppressed in these two alloys. According to **Fig. 1d**, Ni exhibits the largest dislocation loop size but the lowest density, whereas $Ni_{80}Mo_{20}$ shows the smallest loop size and lower loop density compared to NiFe and NiCoV. Comparing the four alloys with distinct degrees of lattice distortion, it is evident that defect cluster size continuously decreases with increasing lattice distortion. However, defect density first increases and then decreases. Thus, moderate lattice distortion can inhibit the growth of large clusters but does not curb the defect density. In contrast, in $Ni_{80}Mo_{20}$, which exhibits the highest degree of lattice distortion, both the defect cluster size and density are reduced, indicating strong suppression of defect evolution.

Additionally, **Supplementary Fig. 11** (previously Supplementary Fig. 13) has been updated to include the high-DPA simulation results, described as follows:

Supplementary Fig. 11 illustrates the defect morphologies in Ni and $Ni_{80}Mo_{20}$ at 10 DPA, along with the evolution of their cluster size distributions as a function of DPA. The results show good agreement with our cascade overlap simulations and irradiation experiments, where large-size defects are found in Ni, whereas isolated point defects and small clusters are dominant in $Ni_{80}Mo_{20}$.

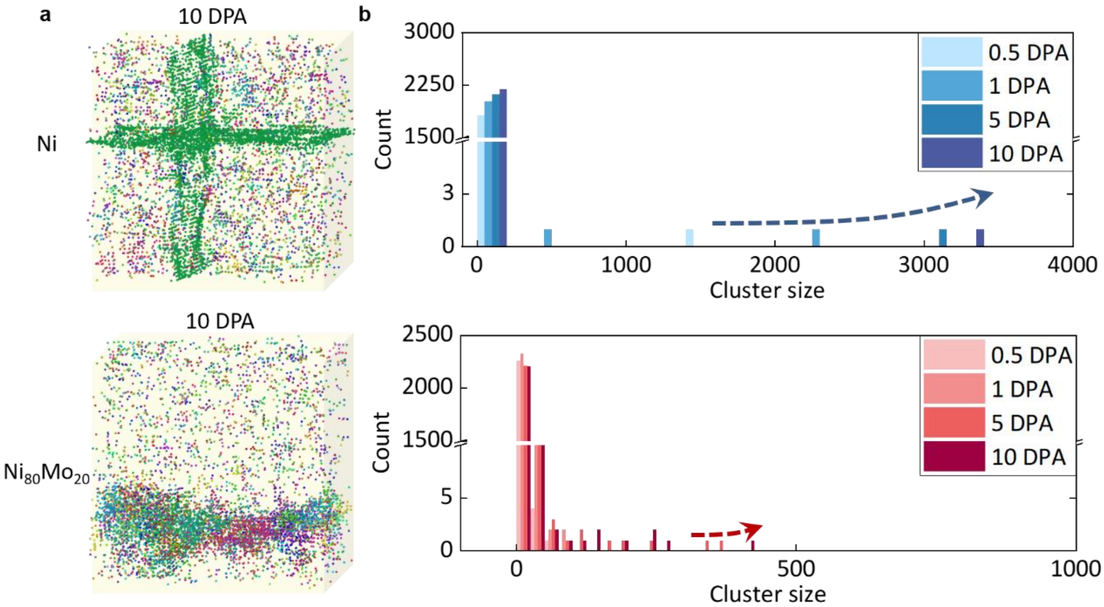

Supplementary Fig. 11. a, Morphology of defects in Ni and $Ni_{80}Mo_{20}$ at 10 DPA. **b**, Evolution of defect cluster size distribution with the increase of DPA. Distinct colors in panel **a** represent different defect-cluster IDs.

<u>Comment 1.2:</u> The modeling results (e.g., Fig. 3) and Figure 4a suggest that introducing distortion decreases the vacancy migration barrier while increasing the interstitial migration barrier, leading to enhanced recombination through barrier overlap. At the same time, the manuscript argues that lattice distortion traps both vacancies and interstitials (i.e., increases

both migration barriers). This appears contradictory. It's noted that in the $Ni_{100-x}Mo_x$ series, increasing Mo content/distortion is shown to increase diffusivity, not reduce it. The authors should carefully reconcile these points and provide one clear mechanism.

<u>Response 1.2:</u> We would like to thank the reviewer for highlighting this point. To clarify, our findings suggest a two-stage effect of lattice distortion on defect transport:

At low-to-moderate distortion levels, vacancy migration barriers decrease while interstitial migration barriers increase, resulting in an overlap of their migration barrier distributions and thereby promoting enhanced recombination (as shown in **Fig. 4a**).

At stronger distortion levels, however, both defects become effectively trapped. Importantly, vacancy trapping does not occur as a result of a further reduction in the migration barrier. Instead, the increased site-energy diversity (σ_{E_0}) generates numerous deep potential wells along the diffusion pathway, leading to strong correlation effects. This correlation makes it unfavorable for vacancies to escape once localized, thereby suppressing their net diffusivity despite lower average migration barriers (**Fig. 3b** and **Supplementary Fig. 5**).

This two-stage mechanism reconciles the modeling with experimental observations: slight-to-moderate distortion promotes recombination by reducing the diffusivity mismatch between interstitials and vacancies, while more substantial distortion suppresses the overall mobility of both defects by enhancing local trapping, thereby inhibiting defect evolution. This trend is consistent with the observation in the $Ni_{100-x}Mo_x$ series. As shown in **Fig. 3d**, vacancy-mediated tracer diffusivity increases with Mo addition at low concentrations but decreases once the Mo content exceeds ~15%. Consistently, the MD trajectories in **Supplementary Fig. 6** reveal that interstitial diffusivity is monotonically suppressed with increasing Mo, whereas vacancy diffusivity follows a non-monotonic pattern—first enhanced, then suppressed.

Accordingly, we have revised the relevant text in the section *Discussion* to present this mechanism more clearly.

MPEAs with extreme chemical disorder are promising due to their inherent resistance to irradiation, which is attributed to disorder-induced slow energy dissipation and defect evolution [18, 29-31]. Such disorder often diminishes the difference between interstitial and vacancy diffusion, as seen in the overlap of their migration barrier distributions, leading to enhanced defect recombination (**Fig. 4a**). As interstitials typically move orders of magnitude faster than vacancies, this overlap suggests that modest lattice distortion in MPEAs tends to slow down interstitials while accelerating vacancies, thereby promoting recombination.

And

Previous investigations have primarily examined alloys with low to moderate lattice distortion, where enhanced vacancy diffusion and suppressed interstitial mobility are dominant features. In contrast, our experiments and simulations reveal that once the lattice distortion exceeds 4%, a condition not previously achieved in FCC materials, both vacancies and interstitials become effectively trapped, yielding smaller and sparser clusters. Notably, although severe lattice distortion lowers the vacancy migration barrier, vacancy diffusion is significantly hindered by the broad distribution of site energies (σ_{E_0}) arising from pronounced 1NN displacements around vacancies, leading to strong correlation effects. This energy heterogeneity results in deep potential wells that locally trap vacancies and impede their long migration.

Taken together, our findings indicate a two-stage effect of lattice distortion on defect evolution: slight-to-moderate distortion enhances recombination by balancing defect mobilities, while severe distortion suppresses defect migration through local trapping. This unified framework reconciles the previously conflicting experimental reports and demonstrates how lattice distortion can be strategically tuned to control defect behavior in irradiated materials, as illustrated in **Fig. 4b**.

Comment 1.3: Diffusion mechanisms are temperature dependent. The manuscript would be strengthened by either providing direct diffusion modeling results at 300 K (to match experimental conditions) or at least a more detailed mechanistic discussion of the differences between the 1000 K modeling results and the 300 K experiments.

Response 1.3: We are grateful to the reviewer for raising this important suggestion. In this study, the displacement cascade simulations were performed at 300 K to match the experimental irradiation conditions, while defect diffusion simulations were conducted at 1000 K to accelerate defect migration and obtain statistically meaningful diffusion events within accessible MD timescales.

Direct diffusion modeling at 300 K is computationally prohibitive because the diffusivity of vacancy is extremely low, and migration events rarely occur within the nanosecond MD window. Nevertheless, the underlying diffusion mechanisms identified at 1000 K are expected to remain operative at 300 K, albeit with much lower frequencies. This trend can be seen in **Fig. 3d**, where the tracer diffusivity D^* was evaluated at different temperatures. The results show that D^* exhibits a consistent compositional trend across all temperatures from 600 to 1000 K, indicating that the same diffusion mechanism is active. Moreover, the trapping behavior becomes more pronounced at lower temperatures due to reduced jump frequencies. Therefore, the relative trends in defect mobility obtained at 1000 K provide meaningful mechanistic insights into how local lattice distortion influences defect transport under irradiation, while maintaining a feasible computational cost.

To clarify this point, we have revised the manuscript to explicitly discuss the connection between the high-temperature diffusion simulations and the 300 K experiments, emphasizing that the 1000 K results are used as a mechanistic reference rather than a direct quantitative comparison.

In the section *Defect accumulation mechanism*:

Defect cluster binding energies provide information on thermodynamics only, which governs stability at equilibrium conditions, while defect kinetics are more relevant to the dynamic defect process under irradiation. To elucidate these kinetic effects, the migration trajectories of individual interstitials and vacancies were analyzed (**Fig. 2c** and **d**, respectively). These trajectories were obtained at 1000 K, a temperature chosen to ensure sufficient migration events for statistically meaningful sampling within accessible MD timescales. Although higher than the experimental irradiation temperature, this choice enables the identification of fundamental diffusion pathways and their dependence on lattice distortion, which are expected to remain operative at lower temperatures despite reduced jump frequencies.

And in the section *Mechanism of defect localization induced by lattice distortions*:

Building on the species-resolved diffusion model with the input of these distributions as detailed in our previous work [45], we calculate the tracer diffusivity mediated by vacancies, as shown in **Fig. 3d**. The results confirm that severe lattice distortion exceeding 4.33% ($Ni_{85}Mo_{15}$) starts to inhibit vacancy diffusion. At this threshold, the effects of vacancy trapping outweigh those of enhanced vacancy jumps, leading to suppressed diffusion. Furthermore, **Fig. 3d** highlights that although the diffusivity increases with temperature due to the thermally activated nature of vacancy migration, the compositional trends remain consistent across the entire temperature range from 600 K to 1000 K. This consistency underscores the critical influence of lattice distortion in governing defect mobility over a wide range of temperatures. Notably, the disparity in diffusivity between alloys with weak and strong lattice distortion becomes more pronounced at lower temperatures, implying that the trapping effect of lattice distortion is even stronger at the 300 K irradiation temperature.

Reviewer 3

The aim of this paper is to tie local lattice distortion to the microstructural evolution of metallic alloys under irradiation. In its current state, the article is not suitable for publication in Nature Communications without substantial revisions for the following reasons.

We deeply appreciate the reviewer's constructive feedback on our study. We acknowledge the comments raised and have addressed each point comprehensively in the responses that follow.

Comment 2.1: *The work does not support several of the claims made. For example, in the introduction the claim is made that, "we demonstrate that superb irradiation-tolerant alloys can be achieved by effectively immobilizing irradiation-induced defects, including interstitials and vacancies, through maximizing lattice distortion effects" yet the work consists of room temperature ion irradiations to a peak damage of 0.43 dpa and modeling up to 0.01 dpa (at non-physical damage rates) with MD and 0.4 dpa with CRA. These temperatures and damage levels are far too low to be able to claim superb irradiation tolerance has been demonstrated as the experimental and simulated conditions are not sufficient to surpass the incubation period before extended defect (e.g., voids) can form. Similarly, it is stated that, "we present a new paradigm to design irradiation-resistant MPEAs through immobilizing both interstitials and vacancies by strategically engineering the degree of lattice distortion," however, many of the concepts presented have been studied at length, including by some of the co-authors, through the Energy Dissipation to Defect Evolution (EDDE) Energy Frontier Research Center EFRC over the last decade (e.g., references 18, 26, https://doi.org/10.1016/j.jnucmat.2019.03.031, https://doi.org/10.1038/ncomms9736).*

Response 2.1: We thank the reviewer for this detailed and constructive assessment. In response, we have strengthened both our experimental and modeling results by extending the irradiation dose to 10 DPA. These new results, presented in **Fig. 1** and **Supplementary Fig. 11**, demonstrate that a high degree of lattice distortion effectively modulates and suppresses defect evolution, confirming its value as a design strategy for irradiation-resistant materials. Specifically, under high-dose irradiation, pure Ni exhibits the formation and growth of large defect clusters, whereas $Ni_{80}Mo_{20}$ with severe lattice distortion continues to display predominantly isolated point defects and small clusters, indicative of strongly suppressed defect aggregation.

Accordingly, we have revised the manuscript as follows:

Fig. 1a shows the cross-sectional distribution of dislocation loops along the depth for all materials post-irradiation, with images obtained under a two-beam condition (g = 200). The region of about 200 nm from the surface was removed due to “flash polishing” thinning. In addition, dislocation loop information from this region was excluded from the statistical analysis to avoid surface effects. Based on SRIM-2013 calculations (using the K-P mode and a displacement threshold energy of 40 eV for all elements), the damage range is approximately 1500 nm, with a peak damage level of about 10 displacement per atom (DPA). The corresponding damage profiles are provided in **Fig. 1b**.

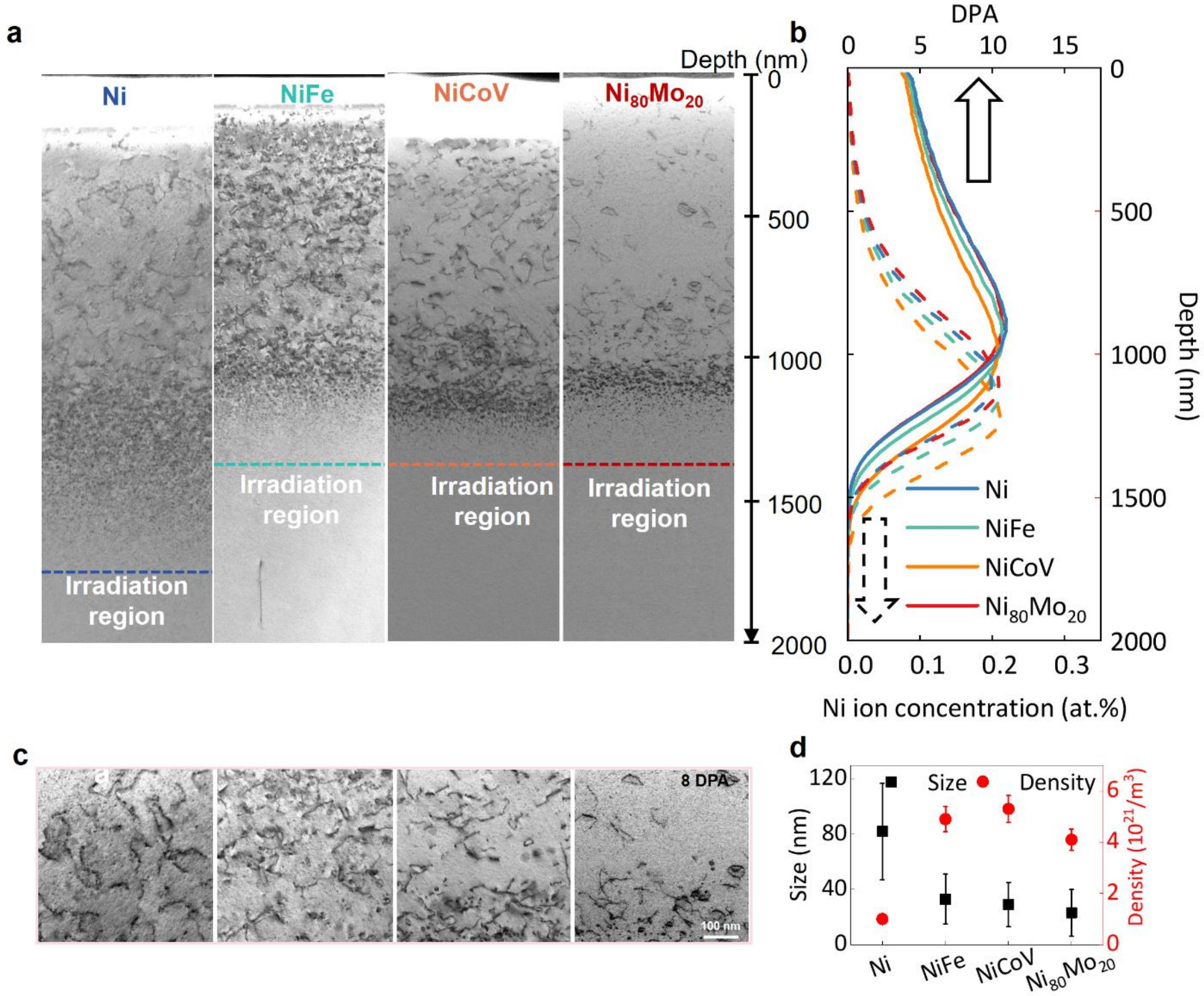

Fig. 1 | Irradiation response of Ni, NiFe, NiCoV, and $Ni_{80}Mo_{20}$ alloys exhibiting various degrees of lattice distortion after exposure to 3 MeV Ni^{+} ions at a fluence of 1×10^{16} ions/cm^2. a, Cross-sectional distribution of dislocation loops along depth after irradiation. **b,** The depth profiles of damage and implanted Ni concentration calculated using the SRIM-2013 software. **c,** Morphological characteristics of dislocation loops at 8 DPA. **d,** Comparison of the average size and density of dislocation loops across the entire irradiated area.

Observations at an irradiation dose of 8 DPA (**Fig. 1c**) reveal that dislocation loops in Ni and NiFe are almost exclusively glissile perfect loops, whereas a fraction of sessile faulted loops is present in NiCoV and $Ni_{80}Mo_{20}$, indicating that the growth of dislocation loops is suppressed in these two alloys. According to **Fig. 1d**, Ni exhibits the largest dislocation loop size but the lowest density, whereas $Ni_{80}Mo_{20}$ shows the smallest loop size and lower loop density compared to NiFe and NiCoV. Comparing the four alloys with distinct degrees of lattice distortion, it is evident that defect cluster size continuously decreases with increasing lattice distortion. However, defect density first increases and then decreases. Thus, moderate lattice distortion can inhibit the growth of large clusters but does not curb the defect density. In contrast, in $Ni_{80}Mo_{20}$, which exhibits the highest degree of lattice distortion, both the defect cluster size and density are reduced, indicating a strong suppression of defect evolution.

And the discussion of CRA simulation in **Supplementary Fig. 11**:

Supplementary Fig. 11 illustrates the defect morphologies in Ni and $Ni_{80}Mo_{20}$ at 10 DPA, along with the evolution of their cluster size distributions as a function of DPA. The results show good agreement with our cascade overlap simulations and irradiation experiments, where large-size defects are found in Ni, while isolated point defects and small clusters are dominant in $Ni_{80}Mo_{20}$.

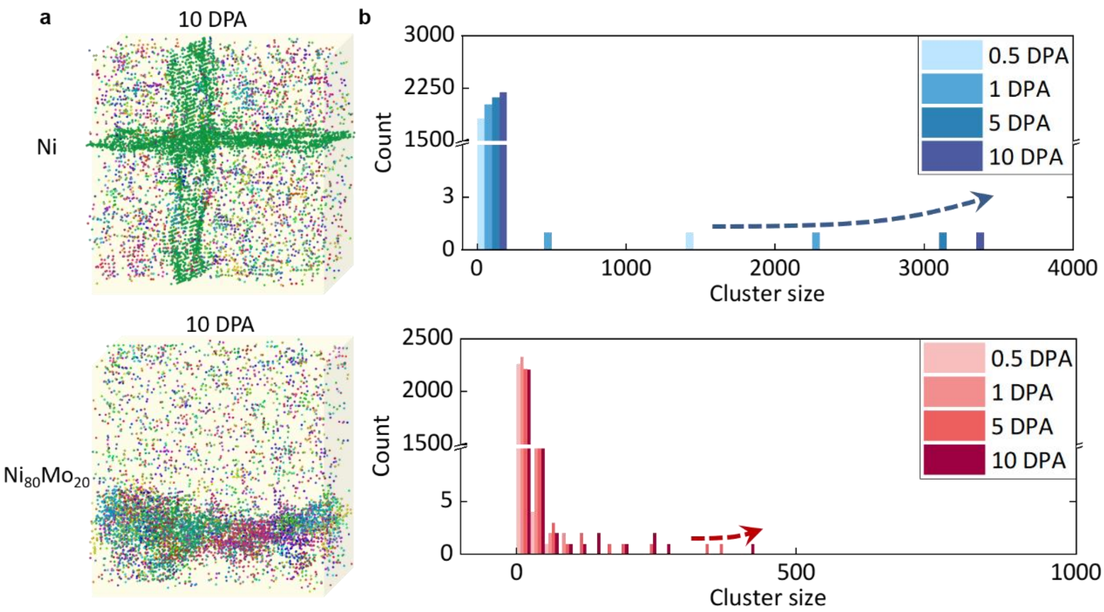

Supplementary Fig. 11. a, Morphology of defects in Ni and $Ni_{80}Mo_{20}$ at 10 DPA. **b**, Evolution of defect cluster size distribution with the increase of DPA. Distinct colors in panel **a** represent different defect-cluster IDs.

Our present finding is fundamentally different from prior results under the EDDE framework. While EDDE has established the critical aspects of chemical disorder–induced energy dissipation in controlling defect mobility, the precise role of disorder remains complex and strongly dependent on the specific alloy constituents. In contrast, our work isolates and demonstrates the effect of lattice distortion alone, independent of chemical complexity, in immobilizing both vacancies and interstitials. This distinction establishes a structural complement to previously reported chemical disorder mechanisms and provides a simplified, composition-independent design route for irradiation-tolerant materials.

In addition, previous studies have primarily explored FCC alloys with slight to moderate lattice distortion, where enhanced vacancy diffusion and reduced interstitial mobility were observed. Our results reveal that by maximizing the lattice distortion, the mobilities of both defect species are simultaneously suppressed—a phenomenon not previously reported. These findings establish a new mechanistic regime of defect dynamics in concentrated alloys.

To emphasize our contribution, we have moved the relevant discussion originally in the supplementary section into the main text, and we have revised the manuscript accordingly as follows:

Irradiation-resistant structural materials are essential for future nuclear energy development. Three proposed pathways for material design include selecting matrix phases with inherent irradiation tolerance, choosing materials with immobile defects, and engineering materials with high sink densities [52]. MPEAs with extreme chemical disorder are promising due to their inherent resistance to irradiation, which is attributed to disorder-induced slow energy dissipation and defect evolution [18, 29-31]. Such disorder often minimizes the difference between interstitial and vacancy diffusion, as seen in the overlap of their migration barrier distributions, leading to enhanced defect recombination (**Fig. 4a**). As interstitials typically move orders of magnitude faster than vacancies, this overlap suggests that modest lattice distortion in MPEAs tends to slow down interstitials while accelerating vacancies, thereby promoting recombination.

Despite these insights, the influence of lattice distortion on direct vacancy diffusion and clustering behavior remains under debate. Some reports describe smaller and denser defect clusters [3, 25], whereas others observe larger clusters under similar irradiation conditions [26, 27]. **Table 2** summarizes the corresponding degrees of lattice distortion, irradiation conditions, and resulting distributions of interstitial and vacancy clusters from these studies.

Our results help reconcile these discrepancies by clarifying the distortion-dependent behavior of defects. At low distortion levels ($\delta<3\%$), the diffusivities of vacancies and interstitials become comparable, promoting efficient Frenkel pair recombination and thus producing smaller yet denser defect clusters. When the distortion increases to a moderate range ($3\%\leqslant\delta<4\%$), interstitial diffusion is further hindered, while the widening of vacancy migration channels lowers the migration barrier, thereby enhancing vacancy mobility and promoting the formation of larger vacancy clusters, as confirmed in **Table 2**.

Table 2 | Summary of experimental observation of the effect of lattice distortion on interstitial clusters and vacancy clusters distribution after irradiation.

Materials	Degrees of lattice distortion	Temperatures & DPAs	Interstitial clusters	Vacancy cluster	Refs.
Ni NiCo NiFe NiFeCoCr NiFeCoCrMn	0 0.24 1.18 1.50 1.80	773 K 60 DPA	Smaller & denser	Smaller & denser	[3]
Ni NiFe NiFeCo NiFeCoCrMn	0 1.18 0.96 1.80	773 K ~53 DPA	N.A.	Smaller & denser	[25]
NiFeCr NiFeCrMn	1.22 1.78	723-973 K 10 DPA	Smaller & denser	No void formation in NiFeCrMn	[53]
NiFeCoCr NiFeCoCrMn NiFeCoCrPd	1.18 1.80 3.65	693 K 50 DPA	Smaller	N.A.	[54]
NiFeCoCrMn NiFeCoCrPd	1.80 3.65	773 K DPA N.A.	Smaller & denser	Larger & lower density	[26]
NiFeCrMn NiFeCrMnAl	1.78 3.51	773 K 50 and 100 DPA	N.A.	Larger & denser in NiFeCrMnAl	[27]

Previous investigations have primarily examined alloys with low to moderate lattice distortion, where enhanced vacancy diffusion and suppressed interstitial mobility are dominant features. In contrast, our experiments and simulations reveal that once the lattice distortion exceeds 4%, a condition not previously achieved in FCC materials, both vacancies and interstitials become effectively trapped, yielding smaller and sparser clusters. Notably, although severe lattice distortion lowers the vacancy migration barrier, vacancy diffusion is significantly hindered by the broad distribution of site energies (σ_{E_0}) arising from pronounced 1NN displacements around vacancies. This energy heterogeneity results in deep potential wells that locally trap vacancies and impede their long migration.

Taken together, our findings indicate a two-stage effect of lattice distortion on defect evolution: slight-to-moderate distortion enhances recombination by balancing defect mobilities, while severe distortion suppresses defect migration through local trapping. This unified framework reconciles the previously conflicting experimental reports and demonstrates how lattice distortion can be strategically tuned to control defect behavior in irradiated materials, as illustrated in **Fig. 4b**.

Conclusion:

In summary, we present a design strategy for irradiation-resistant MPEAs by immobilizing both interstitials and vacancies through strategically engineered lattice distortion. Our findings reveal that while slight distortion impedes interstitial migration and enhances vacancy diffusion, increased lattice distortion restricts the diffusion of both defect types, leading to smaller and sparser defect clusters post-irradiation. Given that lattice distortion is an inherent characteristic of MPEAs, this approach provides a powerful materials design lever for irradiation-resistant materials. Therefore, our research offers a streamlined strategy for MPEA design focused on modulating lattice distortion rather than complex alloy compositions to enhance performance for extreme environment applications.

Comment 2.2: More information is needed regarding the experimental methodology, including the dose rate for the ion irradiation, how the thickness of the TEM lamellae determined (in order to calculate dislocation densities), and how the dpa of the imaged locations was determined. The last point is relevant because the TEM micrographs in Fig 1 appear to show a monotonically decreasing damage depth while the SRIM calculations show

NiFe having a greater depth than Ni80Mo20 and NiCoV having the greatest depth. This is relevant because if the implantation depths are substantially different, then the damage profiles are also substantially different (given similar fluence, material density, and displacement threshold energy which is assumed to be 40 eV for all elements).

Response 2.2: We thank the reviewer for these insightful comments. We have significantly expanded the *Methods* section to include the experimental details. Our specific responses to the points raised are as follows:

1. **Dose rate:** The ion irradiation was conducted with a total fluence of 1×10^{16} ions/cm^2 over a duration of 2.5 hours, corresponding to a dose rate of approximately 1.1×10^{12} ions/cm^2/s.
2. **Thickness determination:** The thickness of the TEM lamellae, which is critical for accurate dislocation density calculation, was determined using a combination of FIB cross-sectional measurements during sample preparation and the Convergent Beam Electron Diffraction (CBED) method within the TEM.
3. **DPA determination:** The dpa values for the imaged regions were determined by correlating the specific depth of the observation area with the depth-dependent damage profile calculated by SRIM simulations. The TEM observations were specifically conducted at a depth range of 450–950 nm. This region was selected to avoid surface effects (0–200 nm) and the injected interstitial peak zone (1100–1300 nm). Based on the SRIM calculations, the local dose in this observed region ranges from 6 to 10 dpa, with an average value of approximately 8 dpa.

The TEM results have been updated with the high-dose irradiation (10 DPA) experiment, which show clearly a consistent damage depth. The 'shallower' damage depth observed in the original low-dose experiment may be a result of the limitation of the defect visibility threshold of the TEM.

We have added the following text to the *Methods* section of the manuscript:

The Ni, NiFe, NiCoV, and $Ni_{80}Mo_{20}$ alloys were fabricated via arc melting followed by drop-casting. Subsequently, the as-cast ingots were subjected to a sequence of thermomechanical treatments. This process included homogenization at 1200° C for 24 h with water quenching, cold rolling to a thickness reduction of ~90%, and final annealing at 800-1100° C, followed by water quenching. The ion irradiation experiments were conducted using the 1.7 MV tandem accelerator at Peking University. Prior to ion irradiation, the samples were sequentially polished by mechanical polishing followed by electropolishing to obtain a mirror-like surface.

The samples were then irradiated at room temperature with 3 MeV Ni ions to a fluence of 1×10^{16} ions/cm^2 and a dose rate of approximately 1.1×10^{12} ions/cm^2/s.

Cross-sectional TEM specimens were prepared using a Thermo Scientific Helios 5UX focused ion beam (FIB) system. The lamellae were sequentially thinned at an accelerating voltage of 30 kV, with beam currents tapering from 0.3 nA to 50 pA, yielding an initial thickness of approximately 160 nm. To eliminate FIB-induced artifacts, such as amorphous layers and defects caused by Ga ion milling, a rapid electrochemical "flash polishing" technique was employed. This process was carried out at 14 V for 80 ms in an electrolyte solution of 4% perchloric acid and 96% ethanol. Consequently, the lamella thickness was reduced to 80-100 nm, suitable for TEM observation. The precise lamella thickness, essential for quantifying dislocation loop densities, was verified using both FIB cross-sectional imaging and the Convergent Beam Electron Diffraction (CBED) method.

Irradiation-induced defects were characterized using an FEI Talos 200X transmission electron microscope. Quantitative analysis of dislocation loops was performed via ImageJ software, with a statistical sample size of approximately 500 dislocation loops per specimen. The damage profile and injected Ni concentration were calculated using SRIM-2013 in K-P mode. The displacement threshold energies were set to 40 eV for all the constituent elements. To ensure the validity of the data, TEM observations were restricted to a depth range of 450–950 nm. This region was strategically selected to avoid the confounding influences of the surface sink effect (0–200 nm) and the injected interstitial peak (1100–1300 nm). According to SRIM predictions, this target region corresponds to a dose range of 6–10 dpa, with a nominal average dose of approximately 8 dpa.

Comment 2.3: From a formatting perspective, the article is overly reliant on supplementary materials. There are 20 references to the supplementary materials, often referring to critical information for the conclusions being drawn. If information is necessary to support the points being made, it needs to be included in the body of the article. Additionally, Supp. Fig. 5 has a typo in the X axis title.

Response 2.3: We would like to thank the reviewer for this precious comment. In the revised manuscript, we have reorganized the content to reduce reliance on the Supplementary Materials and to ensure that all information essential to supporting the main conclusions is presented in the main text.

Specifically, key discussions previously contained in the Supplementary Notes regarding the role of lattice distortion in defect size and distribution have now been incorporated into the main manuscript. In addition, the damage depth profile has been moved to **Fig. 1**.

To streamline the presentation, we have removed **Supplementary Fig. 8** from the original version, as it was not explicitly discussed in the text and is not essential to the conclusions. We have also corrected the typographical error in the X-axis label of **Supplementary Fig. 5** (now **Supplementary Fig. 4**).

We hope these revisions have improved the self-contained clarity of the main article and reduced reliance on the Supplementary Materials.

Reviewer 1

1) This revised manuscript includes new irradiation experiments up to 10 DPA, significantly strengthening the original submission. The new high-dose data demonstrate that the effect of increased "lattice distortion" persists at elevated damage levels and continues to effectively suppress defect cluster size and density.

2) The role of "lattice distortion" in defect evolution is clarified, including the modification of migration barriers and the enhancement of correlation effects. The two-stage mechanism proposed by the authors clearly reconciles the effects on vacancy and interstitial diffusion.

3) As to the discussion of diffusion mechanisms at 1000 K vs. 300 K, it is said that the underlying mechanisms identified at 1000 K remain operative at 300 K, albeit at reduced jump frequencies. Given the broad distribution of migration barriers in concentrated alloys, lowering the temperature effectively selects the lower-barrier diffusion pathways while simultaneously enhancing correlation. Effective diffusion paths and migration modes can change with temperature, e.g., Nature Communications 15, 3879 (2024). The enhanced trapping observed at lower temperatures could originate from such diffusion-mode transitions. It may be helpful to clarify the manuscript, as it more precisely elucidates the temperature-dependent diffusion mechanisms.

Overall, this is an intriguing and technically solid study. By providing mechanistic insight into defect kinetics in chemically disordered alloys, this work offers a new perspective for rationalizing prior conflicting reports and a timely approach to designing radiation-tolerant alloys. The results will be of interest to the broad community, and publication in Nature Communications is therefore recommended!

Response: We thank the reviewer for the positive assessment of our manuscript and for recommending publication. We have incorporated a discussion on low-temperature diffusion in the section relating to **Fig. 3d**. This addition specifically responds to the third point in the comments, as detailed below:

Notably, the disparity in diffusivity between alloys with weak and strong lattice distortion becomes more pronounced at lower temperatures. This trend can be rationalized by the preferential activation of low-barrier migration pathways in MPEAs exhibiting a broad distribution of migration energies, which in turn amplifies vacancy trapping and correlation effects in compositionally complex systems.

Reviewer 3

While qualifying the irradiation tolerance of the reported alloys as "superior" and "superb" is dubious after only modest irradiation doses at room temperature, the revised version of the paper is more relevant with the 10 dpa damage level than the prior 0.43 dpa studied. Similarly, it is difficult to assess just how immobilized the vacancies in the materials are, given that vacancies in most Ni-based alloys are effectively immobile at room temperature already. It remains to be seen whether the trends reported on will hold under reactor-relevant conditions, however the revised experiments and analysis may be included in the body of literature for the basis of discussion and future work.

Response: We thank the reviewer for the positive evaluation of our study. The present work proposes immobilizing defects as an effective strategy for designing irradiation-resistant multicomponent alloys. The agreement between atomistic simulations and experimental observations strengthens this design approach. We agree with the reviewer that future work should incorporate more reactor-relevant conditions, such as neutron irradiation, to further assess the irradiation tolerance of the designed alloys, as well as the design philosophy established in this work. In response, we have removed the word "superior" from the manuscript's title to enhance objectivity. We have also expanded the discussion to include supporting evidence from the literature in the section accompanying **Table 2**, as follows:

Notably, these literature examples, which encompass a range of irradiation temperatures beyond room temperature as in our present work, show defect behaviors consistent with our conclusions, reinforcing the role of distortion in modulating defect mobility and clustering.